Nanotechnology Perceptions
ISSN 1660-6795
www.nano-ntp.com

Electrochemical Performance of Manganese Dioxide (MnO2) Nanoparticles Synthesized by Co-Precipitation Method

D. Thilaga Sundari[1,2], D. Silambarasan[2,3*], R. Sarika[4]

[1]Research Scholar (Reg. no.19231072132008), PG and Research Department of Physics, The M.D.T. Hindu College, Tirunelveli-627010, Tamil Nadu, India
[2]Affiliated to Manonmaniam Sundaranar University, Abishekapatti, Tirunelveli-627012, Tamil Nadu, India
[3]PG and Research Department of Physics, The M.D.T. Hindu College, Tirunelveli-627010, Tamil Nadu, India
[4]Department of Chemistry, Fatima College (Autonomous), Madurai - 625018, Tamil Nadu, India
Email: silambarasan@mdthinducollege.org

Manganese dioxide (MnO2) nanoparticles were synthesized using the co-precipitation method and their structural, optical and electrochemical properties were systematically characterized. Transmission electron microscopy (TEM) revealed that the MnO2 nanoparticles exhibited a well-defined morphology with a uniform size distribution. X-ray diffraction (XRD) analysis confirmed the crystalline nature of the material and Raman spectroscopy further supported the identification of MnO2 phases. Fourier-transform infrared (FTIR) spectroscopy demonstrated the presence of characteristic functional groups, while ultraviolet-visible (UV-Vis) spectroscopy estimated an optical band gap of 2.9 eV. Thermogravimetric analysis (TGA) highlighted the thermal stability of MnO2, with minimal weight loss observed up to 800ºC. Electrochemical properties were evaluated using cyclic voltammetry (CV) and electrochemical impedance spectroscopy (EIS), revealing a high specific capacitance of 236.04 F/g at a scan rate of 10 mV/s. These results suggest that MnO2 nanoparticles possess excellent electrochemical performance making them promising candidates for energy storage applications.

Keywords: Manganese dioxide, co-precipitation method, electrochemical properties, energy storage applications.

1. Introduction

In recent years, considerable efforts have been focused on nanotechnology, particularly on metal oxide nanomaterials [1, 2]. Among all nanomaterials, transition metal oxides at the nanoscale have emerged as significant candidates from both scientific and technological perspectives. Furthermore, transition metal oxides offer distinct advantages, making them one of the most versatile categories of materials with properties that span across various aspects of solid-state physics and materials science [3-5]. MnO_2 among the various transition metal oxides has emerged as a promising candidate as electrode materials for supercapacitors due to its attractive properties, such as low cost, low toxicity, abundant availability, and environmentally friendly nature [6, 7]. Various methods have been employed to prepare MnO_2 nanomaterials, such as co-precipitation [8], electrochemical reductions [9], thermal decomposition [10], microwave-assisted synthesis [11] and hydrothermal [12]. Co-precipitation is widely used technique for the synthesis of metal oxides, as it is simple, cost-effective and does not require high temperatures. This method offers several advantages, including being a simple and rapid preparation technique, allowing for easy control over particle size and composition [13]. Additionally, it provides various options to modify the surface properties of the particles and ensures overall homogeneity. Co-precipitation of various salts (nitrates, sulphates, chlorides, perchlorates etc.) under a fine control of pH by using NaOH or NH_4OH solutions yields corresponding spinel oxide nanoparticles [14].

In this present work, MnO_2 nanoparticles (NPs) were synthesized by co-precipitation method. Various characterizations were carried out to analyze the property of MnO_2. Electrochemical analysis was performed to study the specific capacitance and conductivity of MnO_2 NPs.

2. Experimental

2.1 Materials

Manganese sulphate Monohydrate ($MnSO_4.H_2O$), NaOH pellets (Merck), ethanol (Merck) were purchased. Distilled water was used for the whole process.

2.2 Synthesis

Manganese sulphate monohydrate (0.2 M) was dissolved in 100 ml of distilled water and stirred continuously at a constant temperature of 80°C. NaOH solution was added drop-wise until the pH of the solution reached 12, resulting in a color change to brown. Stirring was continued for an additional 15 minutes at 80°C after the pH reached 12. The precipitate formed was then filtered and washed three times with ethanol. The resultant precipitate was dried at 100°C for 3 hours and calcined at 400°C for 4 hours to remove impurities. The synthesize process is depicted in figure 1.

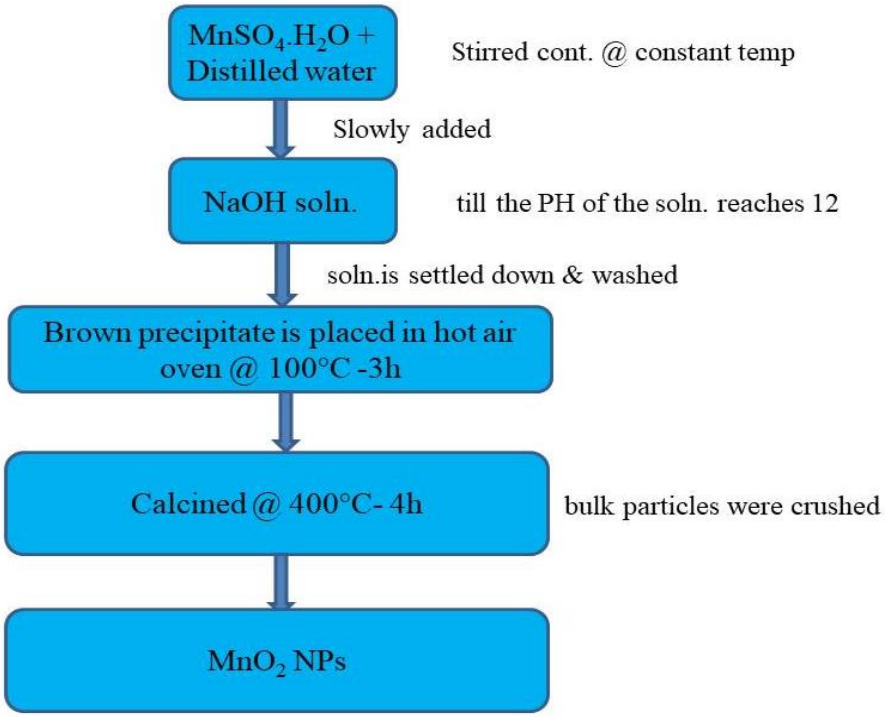

Figure 1: Flow chart of MnO_2 NPs synthesized by co-precipitation method

3. Characterizations

The morphology was investigated by TEM analysis using JEOL JEM 2100 model unit with an accelerating voltage of 200 kV. The XRD analysis was performed on XPERT-PRO diffractometer operating at 40 kV and 30 mA, using Cu Kα radiation in the range 2θ = 10º-80º. The Raman spectroscopy was analyzed by EZ Raman spectrometer. The FTIR spectrum were recorded using Perkin Elmer make spectrum two model in the range of 4000 to 400 cm^{-1} in transmittance mode. UV-visible spectrum were recorded using Perkin Elmer make model lambda 35 in the range of 190-1100 nm. TGA study was carried out using a Perkin Elmer TG/DTA-6300 instrument in the temperature range of 30-800ºC, under ambient conditions with temperature increments of 10ºC/min. The cyclic voltammetry (CV) and electrochemical impedance spectroscopy (EIS) tests were executed by the versa STAT MC model.

4. Results and discussion

4.1. Transmission Electron Microscopy

Figure 2 (a-f) shows the TEM image of the MnO_2 NPs at different scales along with the diffraction pattern. The TEM image demonstrates that the nanoparticles are uniformly distributed with a particle size in the range of 15–20 nm.

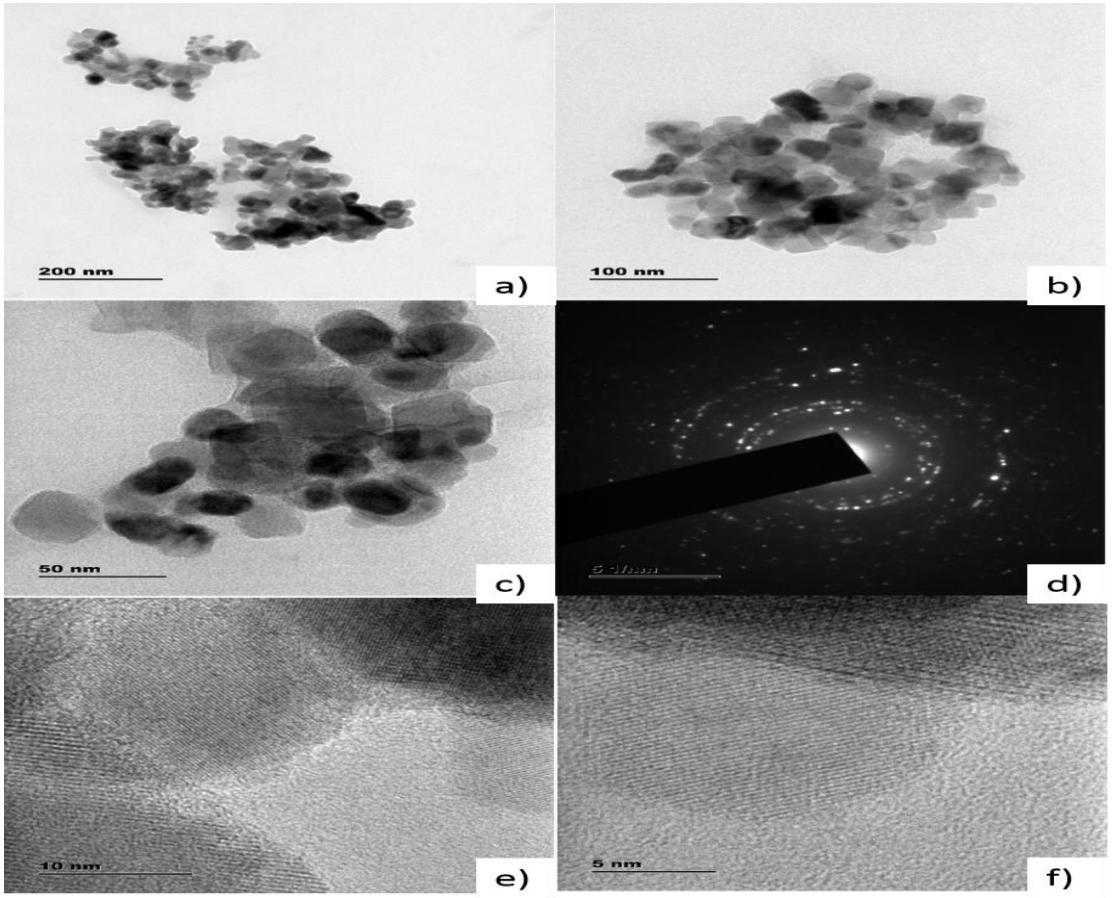

Figure 2: Transmission Electron microscopy of MnO_2 Nanoparticles

4.2. X-Ray Diffraction

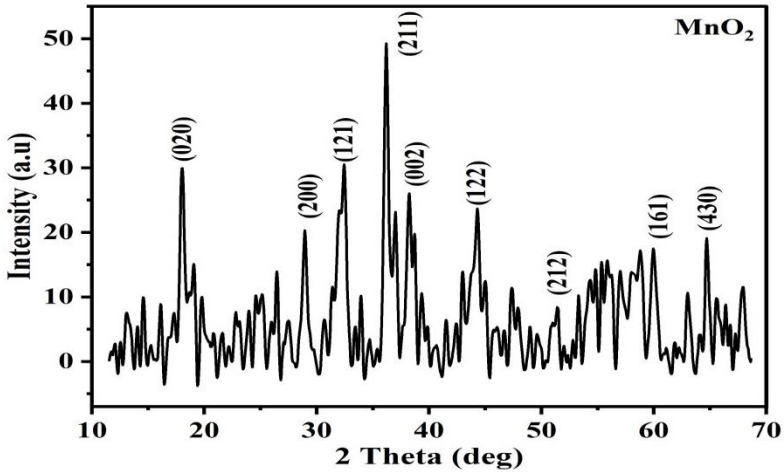

Figure 3: X-Ray diffraction spectrum of MnO_2 NPs

The XRD spectrum of MnO_2 NPs is shown in figure 3. The diffraction pattern of the sample shows the 2θ peaks at 18.05, 28.95, 32.45, 36.20, 38.25, 44.30, 51.35, 59.95 and 64.65°, which specifies the formation of tetragonal phase of MnO_2 NPs. The peaks are indexed to (020), (200), (121), (211), (002), (122), (212), (161) and (430) planes respectively, which are interrelated with JCPDS card (file no: 14-644) [15, 16]. Debye Scherrer equation was used to calculate the crystallite size of the sample [8]. The calculated crystallite size of MnO_2 NPs is 15.4 nm.

4.3. Raman Spectroscopy

Figure 4 displays the Raman spectrum of MnO_2 NPs. The prominent peak at 634 cm^{-1} is accredited to symmetrical Mn–O stretching vibrations of the MnO_6 octahedral and is assigned to the spectroscopic modes, which indicate a well-developed tetragonal structure [17, 18].

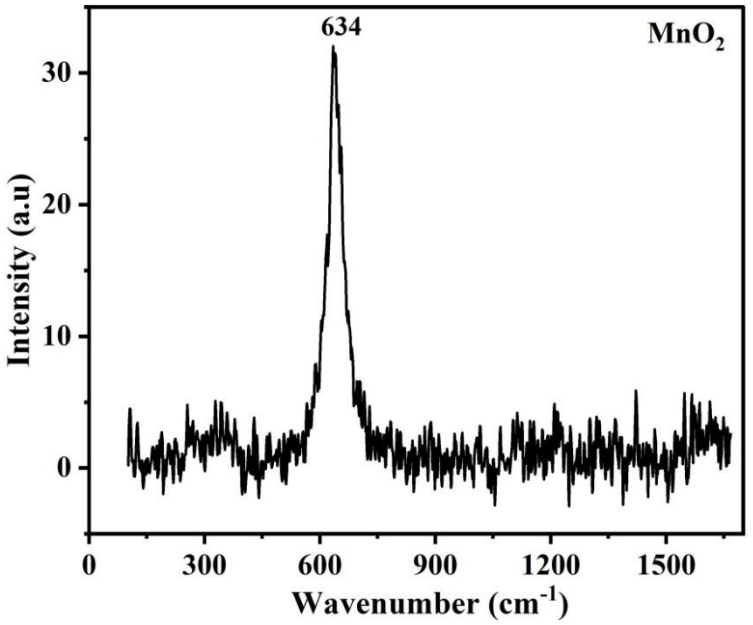

Figure 4: Raman spectrum of MnO_2 NPs

4.4. FTIR Spectroscopy

The FTIR spectrum of MnO_2 NPs is illustrated in figure 5. The FTIR spectrum was used to identify the functional groups present in the sample. The broad band at 3433 cm^{-1} is attributed to the O-H stretching vibrations of hydrogen-bonded surface water molecules and hydroxyl groups [19]. The band at 2925 and 2023 cm^{-1} corresponds to C-H stretching vibrations [15]. The bands at 1621, 1380 and 1106 cm^{-1} is assigned to the existence of many residual O–H groups, indicating that the traces of adsorbed water vibrate in the O–H model [20, 21]. Oxides and hydroxides of metal nanoparticles generally gives absorption peak in the finger print region i.e. below wavelength of 1000 nm arising from inter-atomic vibrations [13]. The bands at 620 cm^{-1} and 523 cm^{-1} are characteristic of O–Mn–O stretching vibrations, indicating the presence of MnO_2 in the sample [22, 23].

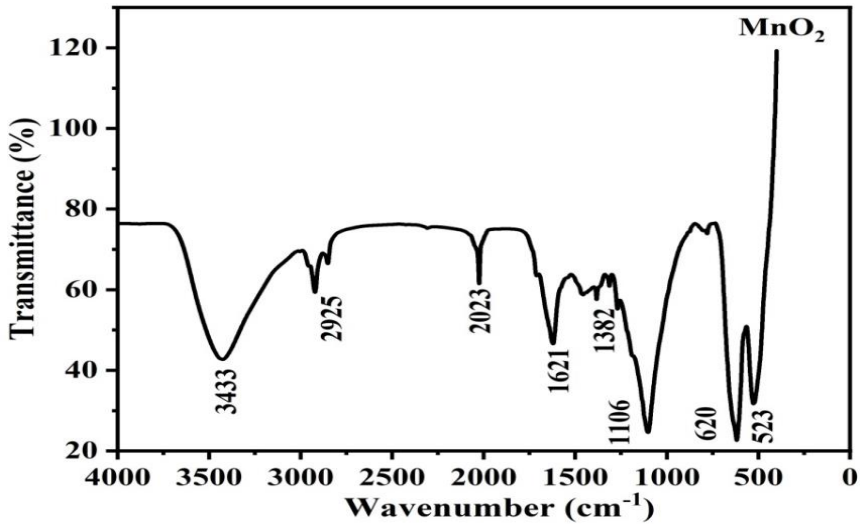

Figure 5: FTIR spectrum of MnO_2 NPs

4.5. UV-Visible Spectroscopy

Figure 6(a) demostrates the UV-Vis absorption spectrum of MnO_2 NPs. The sample shows absorption peaks at 240 nm [24] and 398 nm [25] for MnO_2 NPs. The particle under study has an absorption coefficient (α) obeying the following relation for high photon energies (hυ),

$h\upsilon\alpha = (h\upsilon - E_g)^{1/2}$

where, E_g is the optical band gap, h is the Planck's constant and υ is the frequency of the incident photons [26]. Figure 6(b) shows the optical band gap using tauc plot of the MnO_2 NPs. The optical energy band gap (Eg) was estimated as 2.9 eV.

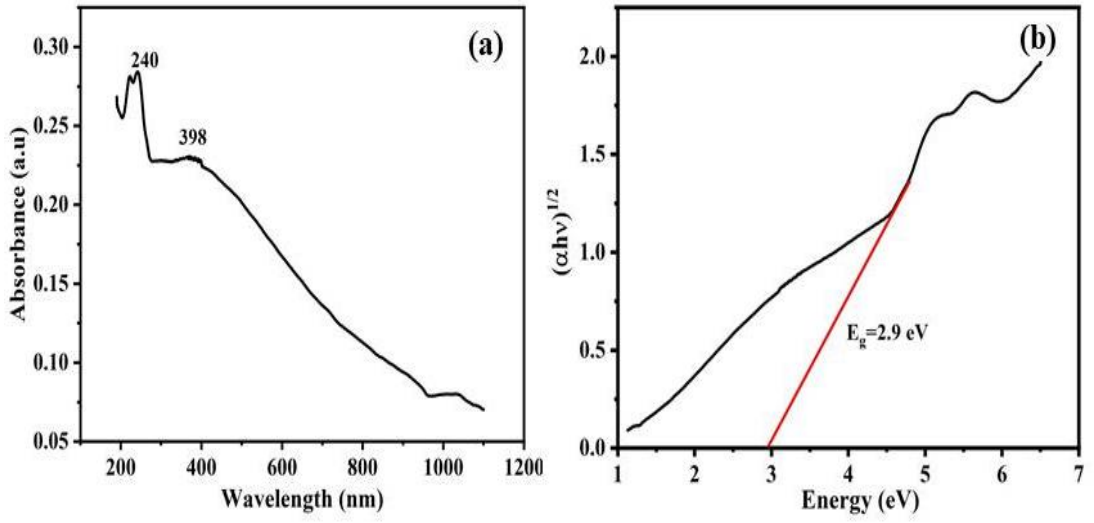

Figure 6: (a) UV–Vis spectroscopy and (b) Tauc plot of MnO_2 NPs

4.6. Thermogravimetric Analysis

Figure 7 exhibits the TGA spectrum of MnO_2 NPs. It is observed that, weight loss before 200ºC is due to the adsorption of water molecules. The weight loss observed above 450ºC for the sample is due to the phase transition of MnO_2 to Mn_2O_3 or Mn_3O_4 [27, 28]. The total weight loss till 800ºC is 4.6% for MnO_2. This relatively small weight loss indicates that MnO_2 is thermally stable even when heated to high temperatures (800ºC).

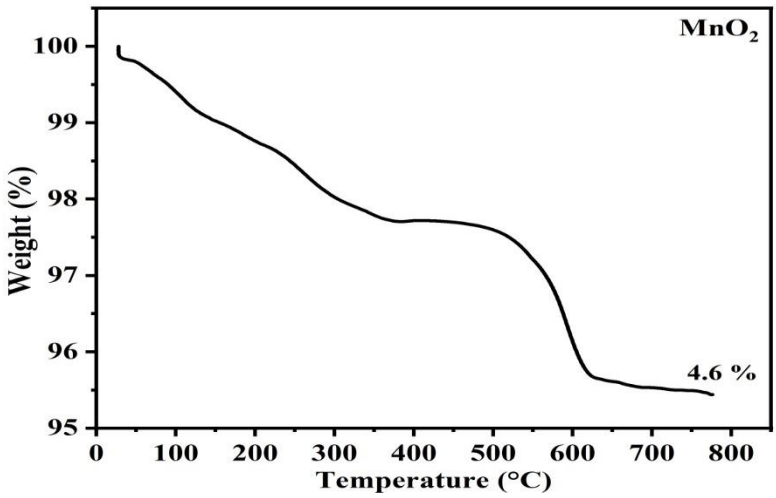

Figure 7: TGA spectrum of MnO_2 NPs

4.7. Electrochemical characterization

The electrochemical properties of MnO_2 can be effectively characterized using CV and EIS, providing insights into its capacitive behaviour and charge storage mechanisms. Cyclic voltammetry studies was performed with the Calomel as reference electrode, platinum as a counter electrode and the sample as working electrode in KOH solution. Figure 8 shows the CV curve and Nyquist plot of MnO_2 NPs.

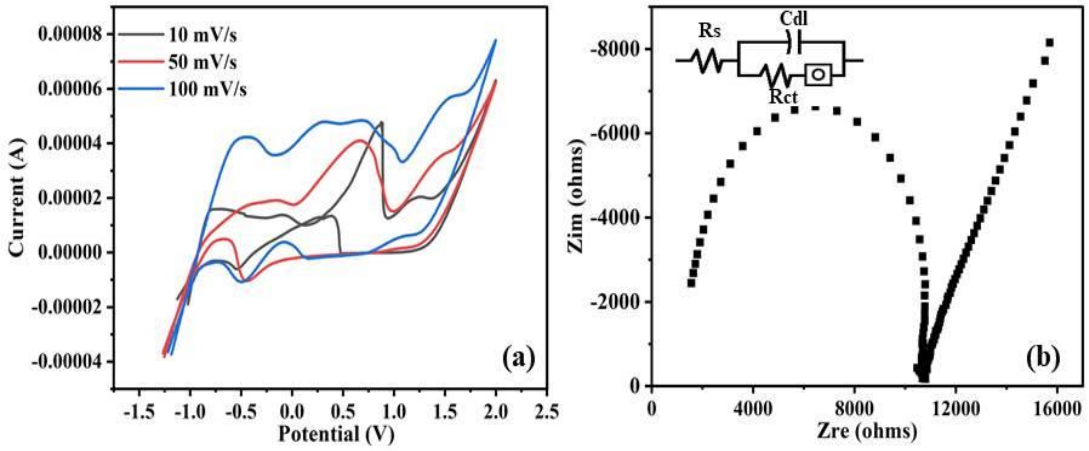

Figure 8: (a) CV curves (b) Nyquist plot and equivalent circuit of MnO_2 NPs

The specific capacitance was calculated by the formula given below:

$$C_{sp} = \frac{1}{2m.v.\Delta V} \int I(V)dV$$

'where 'Csp' is the specific capacitance, 'm' is the mass of active materials grafted on the electrode surface, 'I (V)' is the current on the CV curve, 'υ' is the potential scan rate, and 'ΔV' is potential window [29, 30]. The obtained specific capacitance calculated using the CV curves at scan rates 10, 50 and 100 mV/s is 236.04, 47.20 and 21.80 F/g, respectively. These results indicate that the specific capacitance decreases with increasing scan rate. At lower scan rates, the electrolyte ions have sufficient time to diffuse into the electrode pores, allowing more active sites to participate in the redox reactions. In contrast, at higher scan rates, the diffusion process becomes limited, reducing the effective utilization of the electrode material [31, 32].

EIS was performed to understand the charge transfer and resistive components of the MnO_2 electrode. The Nyquist plot (figure 8b) showed a semicircle in the high-frequency region and a straight line in the low-frequency region. The equivalent circuit (figure 8b inset) used for fitting the EIS data consists of the following elements: Solution resistance (Rs) represents the resistance of the electrolyte and electrode, Charge transfer resistance (Rct) represents the resistance at the electrode-electrolyte interface, Double-layer capacitance (Cdl) is the capacitive behaviour of the electrode and Warburg impedance (O) signifies the diffusion of ions within the electrode material. The semicircle in the high-frequency region corresponds to Rct, while the straight line in the low-frequency region represents the diffusion-controlled Warburg behaviour. The Rs and Rct indicate ionic conductivity and charge transfer kinetics, essential for high-performance energy storage [33,34]. On the whole, the synthesized MnO_2 NPs is suitable for energy storage applications.

5. Conclusion

MnO_2 nanoparticle was successfully synthesized by co-precipitation method. TEM images show the particle size in the range of 15-20 nm. XRD and Raman confirm the tetragonal structure of MnO_2. FTIR spectrum reveals the presence of functional group. The optical energy band gap (Eg) was estimated as 2.9 eV. The maximum specific capacitance was observed 236.04 F/g at a scan rate of 10 mV/s. Hence, MnO_2 NPs is a promising material for electrochemical applications.

Acknowledgements

The authors acknowledge, Dr. K. Subramonian, Associate Professor, Department of Botony, The M.D.T. Hindu College, Tirunelveli, Tamil Nadu, India for granting laboratory facilities.

References

1. N. Tsolekile, S. Parani, M.C. Matoetoe, S.P. Songca, O.S. Oluwafemi, Evolution of Ternary I-III–VI QDs: Synthesis, Characterization And Application, Nano-Struct.Nano-Objects, 12 (2017) 46–56.
2. Akbari, M. Amini, A. Tarassoli, B. Eftekhari-Sis, N. Ghasemian, E. Jabbari, Transition Metal Oxide Nanoparticles As Efficient Catalysts in Oxidation Reactions, Nano-Struct. Nano-Objects, 14 (2018) 19–48.

3. H. Osgood, S.V. Devaguptapu, H. Xu, J. Cho, G. Wu, Transition Metal (Fe Co, Ni,and Mn) Oxides for Oxygen Reduction and Evolution bifunctional catalysts in alka-line media, Nano Today, 11 (2016) 601–625.
4. V. Polshettiwar, B. Baruwati, R.S. Varma, Self-Assembly of Metal Oxides Into Three-Dimensional Nanostructures: Synthesis And Application In Catalysis, ACS Nano, 3 (2009) 728–736.
5. M.M. Najafpour, M. Amini, M. Ashrafi, Lessons From Metal Oxides to Find Why Nature Selected Manganese And Calcium For Water Oxidation, Int. J. Hydrogen Energy, 42 (2017) 8539–8544.
6. D.P. Dubal, R. Holze, All-Solid-State Flexible Thin Film Supercapacitor Based on Mn3O4 Stacked Nanosheets With Gel Electrolyte, Energy, 51 (2013) 407-412.
7. A. Kumar, A. Sanger, A. Kumar, Y. Kumar, R. Chandra, An Efficient α-MnO2 Nanorods Forests Electrode for Electrochemical Capacitors With Neutral Aqueous Electrolytes, Electrochim. Acta, 220 (2016) 712-720.
8. H.R. Mahmoud, Highly Dispersed Cr2O3–ZrO2 Binary Oxide Nanomaterials as Novel Catalysts for Ethanol Conversion, J. Mol. Catal. A, 392 (2014) 216–222.
9. D.M. Clifford, C.E. Castano, J.V. Rojas, Supported Transition Metal Nanomaterials: Nanocomposites Synthesized By Ionizing Radiation, Radiat. Phys. Chem., 132 (2017) 52–64.
10. X. Zhao, F. Zhang, S. Xu, D.G. Evans, X. Duan, From Layered Double Hydroxides To ZnO-Based Mixed Metal Oxides By Thermal Decomposition: Transformation Mechanism And UV-Blocking Properties of The Product, Chem. Mater., 22 (2010) 3933–3942.
11. L. Gu, L. Qian, Y. Lei, Y. Wang, J. Li, H. Yuan, D. Xiao, Microwave-assisted Synthesis of Nanosphere-Like NiCo2O4 Consisting of Porous Nanosheets And Its Application In Electro-Catalytic Oxidation Of Methanol, J. Power Sources, 261 (2014) 317–323.
12. J.R. Kim, K.Y. Lee, M.J. Suh, S.K. Ihm, Ceria-zirconia mixed oxide prepared bycontinuous hydrothermal synthesis in supercritical water as catalyst support, Catal.Today, 185 (2012) 25–34.
13. Harish Kumar, Manisha, Poonam Sangwan, Synthesis and Characterization of MnO2 Nanoparticles using Co-precipitation Technique, International Journal of Chemistry and Chemical Engineering, 3 (2013) 155-160.
14. Thais Cavalcante de Souza, Andréa Fernanda de Santana Costa, Gloria Maria Vinhas, Leonie Asfora Sarubbo, Synthesis of Iron Oxides and Influence on Final Sizes and Distribution in Bacterial Cellulose Applications, Polymers, 15 (2023) 3284-1-3284-18.
15. R. Manjula, M. Thenmozhi, S. Thilagavathi, R. Srinivasan, A. Kathirvel, Green Synthesis And Characterization of Manganese Oxide Nanoparticles From Gardenia Resinifera Leaves, Materials Today: Proceedings, 26 (2020) 3559-3563.
16. S. Ganeshan, P. Ramasundari, A. Elangovan, G. Arivazhagan, R. Vijayalakshmi, Synthesis And Characterization of MnO2 Nanoparticles: Study of Structural And Optical Properties, Int J Sci Res Phys Appl Sci., 5 (2017) 5-8.
17. G. Marciniuk, R.T. Ferreira, A.V. Pedroso, A.S. Ribas, R.A. Ribeiro, S.R. De Lazaro, E.C. De Souza, L.F. Marchesi, J.R. Garcia, Enhancing Hydrothermal Formation of α-MnO2 Nanoneedles Over Nanographite Structures Obtained By Electrochemical Exfoliation, Bulletin of Materials Science, 44 (2021) 62-1-62-11.
18. T. Gao, H. Fjellvag, P. Norby, A Comparison Study on Raman Scattering Properties Of α-and β-MnO2, Anal. Chim. Acta 648 (2014) 235–239.
19. M. Pang, G. Long, S. Jiang, Y. Ji, W. Han, B. Wang, X. Liu, Y. Xi, Rapid Synthesis of Graphene/Amorphous A-MnO2 Composite With Enhanced Electrochemical Performance For Electrochemical Capacitor, Mater. Sci. Eng., B, 194 (2015) 41-47.
20. Yogesh Kumar, Seema Chopra, A. Gupta, Y. Kumar, S.J. Uke, S.P. Mardikar, Low Temperature Synthesis of MnO2 Nanostructures For Supercapacitor Application, Materials Science for

Energy Technologies, 3(2020) 566-574.
21. D. Rui, Y. Kun-De, M. Yuan-Liang, L. Bo, A Reliable Acoustic Path: Physical Properties And A Source Localization Method, Chin. Phys. B, 21(2012) 124301-1-124301-15.
22. D. Jaganyi, M. Altaf, I. Wekesa, Synthesis and Characterization of Whisker-Shaped MnO2 Nanostructure At Room Temperature, Appl. Nanosci., 3 (2013) 329– 333.
23. Md. Abu Bakar Siddique, Ummey Hafsa Bithi, Aninda Nafis Ahmed, M.A. Gafur, Akter Hossain Reaz, Chanchal Kumar Roy, Md. Mominul Islam, Shakhawat H. Firoz, Preparation of Manganese Oxide Nanoparticles with Enhanced Capacitive Properties Utilizing Gel Formation Method, CS Omega, 51 (2022) 48007–48017.
24. Y.G. Lim, H.J. Kim, K. Park, A Novel Method For Synthesizing Manganese Dioxide Nanoparticles Using Diethylenetriamine Penta Acetic Acid as a Metal Ion Chelator, J. Ind. Eng. Chem., 93 (2021) 407-414.
25. Vahid Hoseinpour, Mahsa Souri, Nasser Ghaemi, Green Synthesis, Characterization, and Photocatalytic Activity Of Manganese Dioxide Nanoparticles, Micro & Nano Letters, 13 (2018) 1560-1563.
26. Muhammad Farooq Warsi, Muhammad Bilal, Sonia Zulfiqar, Muhammad Usman Khalid, Philips O Agboola, Imran Shakir, Enhanced Visible Light Driven Photocatalytic Activity of MnO2 Nanomaterials and Their Hybrid Structure With Carbon Nanotubes, Mater. Res. Express, 7 (2020) 105015-1-105015.
27. Ravinder N. Reddy, Ramana G. Reddy, Synthesis and Electrochemical Characterization of Amorphous MnO2 Electrochemical Capacitor Electrode Material, J. Power Sources, 132 (2004) 315–320.
28. Y. Munaiah, B.G. Raj, T.P. Kumar, P. Ragupathy, Facile Synthesis of Hollow Sphere Amorphous MnO2, the Formation Mechanism, Morphology and Effect of a Bivalent Cation-Containing Electrolyte On Its Supercapacitive Behavior, J. Mater. Chem. A, 1 (2013) 4300-4306.
29. M. Zhang, X. Dai, C. Zhang, Y. Fuan, D. Yang, J. Li, High Specific Capacitance of the Electrodeposited MnO2 on Porous Foam Nickel Soaked in Alcohol and its Dependence on Precursor Concentration, Materials, 13 (2020) 181-1-181-12.
30. W. Yang, L. He, X. Tian, M. Yan, H. Yuan, X. Liao, J. Meng, Z. Hao, L. Mai, Carbon-MEMS-based Alternating Stacked MoS2@RGO-CNT Micro-Supercapacitor With High Capacitance And Energy Density, Small, 13 (2017) 1–8.
31. Prasenjit Haldar, Sudipta Biswas, Vikas Sharma, Amreesh Chandra, Understanding the Origin of Magnetic Field Dependent Specific Capacitance in Mn3O4 Nanoparticle Based Supercapacitors, J. Electrochem. Soc., 165 (2018) A3230-A3239.
32. J. Wang, S. Dong, B. Ding, Y. Wang, X. Hao, H. Dou, Y. Xia, X. Zhang, Pseudocapacitive Materials For Electrochemical Capacitors: From Rational Synthesis to Capacitance Optimization, Natl. Sci. Rev., 4 (2017) 71-79.
33. Subir Paul, Asmita Ghosh, Electrochemical characterization of MnO2 as electrocatalytic energy material for fuel cell electrode, J Fuel Chem Technol., 43 (2015) 344□351.
34. Seung-Beom Yoon, Jong-Pil Jegal, Kwang Chul Roh, and Kwang-Bum Kim, Electrochemical Impedance Spectroscopic Investigation of Sodium Ion Diffusion in MnO2 Using a Constant Phase Element Active in Desired Frequency Ranges, J. Electrochem. Soc., 161 (2014) H207-H213.